Journal of the Ceramic Society of Japan 118 [7] 579-586 2010 Paper

The inhibitory effects of inulin biopolymers on the seeded growth of hydroxyapatite

Özlem DOGAN, Mualla ÖNER† and Özge CINEL

Yıldız Technical University, Chemical Engineering Department, Davutpasa 34210 Istanbul, Turkey

In this work crystallization kinetics of hydroxyapatite (HAP) were investigated in the presence of a biodegradable, environmentally friendly polysaccharide-based polycarboxylate, carboxymethyl inulin (CMI), under strictly controlled temperature, pH, and atmospheric conditions. The constant-composition method has been used to study the influence of biopolymers of crystal growth of HAP, on HAP seed crystals at pH 7.4 and 37°C. The results indicate that polymer concentration and the larger number of negatively charged functional groups markedly affect the growth rate. Biopolymer affects the coherence length of the crystalline domain. The decrease in growth rates was substantiated by SEM which showed smaller crystal sizes as a function of increasing carboxylation degree of the CMI and its concentration.

©2010 The Ceramic Society of Japan. All rights reserved.

Key-words : Hydroxyapatite, Biopolymer, Crystallization, Biomineralization

[Received February 15, 2010; Accepted May 20, 2010]

1. Introduction

Hydroxyapatite ($Ca_5(PO_4)_3OH$, HAP) is a compound of great interest because it is the main inorganic constituent of human bones, teeth and soft tissues.[1)] As a compound with structural and chemical resemblance of bone mineral, HAP is of particular importance in the field of biomaterials. The properties that make HAP superior as a biomaterial in contrast to the metals or bioinert ceramics are biocompatibility with hard and soft tissues, bioactivity and absence of toxicity.[2)] The precipitation and dissolution of calcium phosphate salts have many important biological applications.[3)] HAP is a well known bioceramic material used as an ocular implant, scaffold matrix for tissue engineering, bone substitute for filling bone defects or coating metallic implants, thus allowing a better post-surgical recovery due to its chemical and biological similarity with natural bone mineral. Under physiological conditions the most stable calcium phosphate phase is HAP.[4)] The controlled nucleation and growth of HAP is essential for the study of hard tissues calcification and in many undesirable cases of pathological mineralization such as articular cartilage, dental caries, and stones in gall bladder and kidney.[5)–7)]

The size of HAP crystals has primary importance for the biomedical area because biodegradable polymers can be mixed with nano particles to make composites. Nano-sized HAP exhibited better bioactivity than coarser crystals. It is also believed that nanostructured HAP can improve the sintering kinetics because of higher surface area and subsequently improve mechanical properties.[8)] The use of nano-particulate materials to attain more superior mechanical properties has been proposed to solve insufficient strength and durability of the HAP.

The molecular control of inorganic crystallization by organic substances is a key technology for the fabrication of novel materials that has recently received a considerable amount of attention.[9),10)] This process mimics biological mineralization in which a preorganized organic phase provides a niche for inorganic crystals to nucleate and grow. The biological synthesis of inorganic solids often yields materials of uniform size, unusual habit, organized texture and defined structure and composition under moderate conditions of supersaturation and temperature.[11),12)] One problem in nucleation and crystal growth, of considerable interest in biological situations, concerns the way in which certain polymers affect crystallization from supersaturated solutions of inorganic salts.[13),14)]

The purpose of this investigation was to study the selective effect of carboxymethylinulin (CMI, **Fig. 1**) on the crystallization kinetics of HAP. Previous works showed that CMI influences the spontaneous precipitation of calcium carbonate[15)–17)] and calcium oxalate.[15),18)] CMI is also reported as a silica scale remover.[19)]

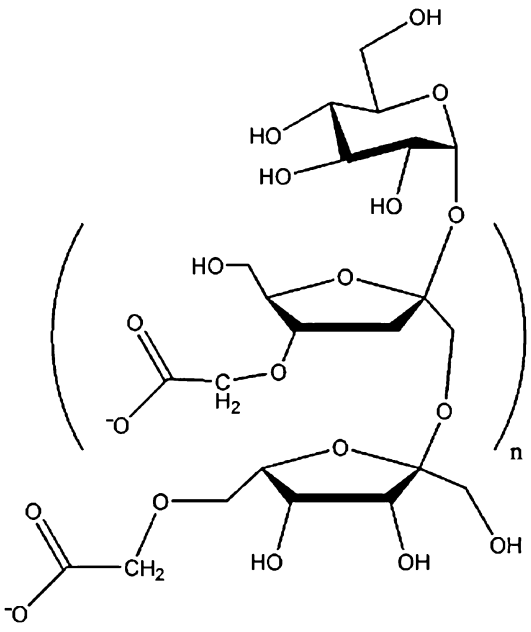

Fig. 1. Schematic structures of carboxymethylinulin.

† Corresponding author: M. Öner; E-mail: oner@yildiz.edu.tr

©2010 The Ceramic Society of Japan

Table 1. The characterization of biopolymers

Polymer	Mn (Da)	Mw (Da)	Mw/Mn	Mz (Da)
CMI15	3022	3927	1.3	5.332
CMI20	2450	3524	1.4	5.200
CMI25	3005	4699	1.5	6.942

CMI is produced from a chemical reaction with a plant-derived biopolymer and select reagents.[20] This biopolymer, inulin,[21] is extracted from the roots of the chicory plant (dry matter content: 20–25%, inulin content: 14.9–18.3%). CMI has been investigated in a series for acute toxicity. Among other attractive attributes of CMI, its inherent biodegradability and non-toxicity are most prominent.[22]

2. Experimental procedure

2.1 Materials

Calcium chloride and dipotassium hydrogen phosphate (reagent grade) were from J. T. Baker. CMI (all three grades) was from thermPhos, Switzerland as Dequest DPB-116AB (where AB = 15 for CMI-15, AB = 20 for CMI-20 and AB = 25 for CMI-25). The number AB also indicates the degree of substitution (DS). DS is defined as the average number of carboxylate moieties per fructose unit. For example, for CMI-15, DS = 1.5; for CMI-20, DS = 2.0; for CMI-25, DS = 2.5. Viscotek TDA 302 detector system with refractive index (660 nm), right angle light scattering (670 nm) and differential viscometer detectors was used for on-line Size-exclusion chromatography (SEC) signal detection.

HPLC pump, degasser and autosampler were built-in Viscotek GPCmax VE 2001 pump system, which is connected to the detectors. OmniSEC 4.1 software was used for the acquisition and analysis of SEC data. Viscotek triple detector array was calibrated using PEO peak in a mobile phase of PBS at 0.7 mL/min flow rate. TSK G3000PWxl column in the dimensions of 300 mm length was used for molecular weight determination. The data are given in **Table 1**.

2.2 Preparation of seed

Two hundred fifty milliliters of 0.50 mol/L $CaCl_2$ and 0.10 mol/L KOH to adjust the pH at 9.5 were added to the reaction vessel, which was thermostated at 70°C. This solution was mixed with 0.30 mol/L dipotassium hydrogen phosphate solution, which was added dropwise over a period of 2 h. During the precipitation process, the pH was kept constant between 9.0 and 9.5 by small additions of KOH solution. The reactor was stirred with a magnetic stirrer at approximately 550 rpm. The presaturated nitrogen gas was introduced into the stirred solution during reaction to ensure a CO_2 free atmosphere. The resulting seed suspension was separated and refluxed for five hours in its supersaturated solution, aged for one month at 37°C, while pH was kept at about 7. At the end of this period, the crystals were filtered, dried at room temperature and stored in a desiccator.

X-ray diffraction analysis of the HAP samples was carried out by means Phillips Panalytical X'ert Pro powder diffractometer operating with Cu Kα radiation in operating at 40 mA and 40 kV. The 2θ range was from 10 to 60° at scan rate of 0.020° step^{-1}. Purity of the seed samples was also tested FTIR spectral analysis. The crystallite morphology of samples was analyzed by scanning electron microscopy (JEOL-FEG-SEM). The specific surface area (SSA) of the HAP crystals was determined by nitrogen sorption isotherms according to multiple-point BET (Brunauer, Emmett and Teller) method using a continuous flow apparatus (Costech Sorptometer 1042). The crystals were outgassed for 24 h at 40°C. The SSA determined by multiple-point nitrogen adsorption was 26.63 m^2/g. Particle size of the crystals was investigated using SEM.

2.3 Crystal growth experiments

Crystal growth experiments were performed at constant composition conditions. The ability to measure quantitatively the rates of mineralization at constant thermodynamic driving forces is one of the most important advantages of the constant composition kinetic methods.[23]

In a typical constant-composition crystal growth experiment, stable supersaturated solutions of calcium phosphate with a molar ratio of $Ca_T/P_T = 1.67$ were prepared in a water-jacketed reactor. The total molar concentration of calcium, Ca_T was 5×10^{-4} mol/L with calcium/phosphate molar ratio 1.67. It should be noted that this solution was undersaturated with respect to other calcium phosphate phases such as OCP (octacalcium phosphate) and DCPD (dicalcium phosphate dihydrate).[6),24),25)] The pH was adjusted to the required value by the addition of dilute potassium hydroxide solution. Following the pH adjustment and verification of the stability of the supersaturated solution for at least 2 h, a quantity of 40 mg/L HAP seed crystal was added to the solution. The biopolymer solutions were added to the reaction medium prior to the inoculation with seed crystals of HAP. The crystal growth was started immediately after the introduction of HAP seed crystals into the solutions and no induction time was observed both in the absence and presence of polymer. Following the addition of seed crystals, the first tendency for pH decrease by 0.005, triggered the addition of titrant solutions which was controlled by means of a pH-stat (Radiometer pH-Stat Titrator PHM290, Auto-Burets ABU901).The crystal growth was monitored by the addition of titrant solutions as a function of time from the two mechanically coupled automatic burettes. Throughout the course of the seeded growth experiments, the pH of the working solution and the added volume of titrants as a function of time were recorded.

The concentrations of the titrants were such that their addition exactly compensated for the changes in anion and cation concentrations, during the precipitation. During crystal growth a pH-stat apparatus senses decreasing pH and causes the double burette system to respond by adding calcium chloride, dipotassium hydrogen phosphate and potassium hydroxide titrant solutions replacing calcium and phosphate ions lost to crystal growth, keeping pH and solution composition constant. Since it is desired to investigate the influence of biopolymer on crystal growth they were included in the titrant to compensate for dilution effects. Addition of the potassium chloride inert electrolyte in the supersaturated solution and the titrants enabled the ionic strength during crystal growth ($IS = 6.5 \times 10^{-3}$ mol/L, pH 7.4). The burettes compositions were given below:

Burette 1

$$[Ca]_{tit} = 10Ca_T + n_B Ca_T$$

Burette 2

$$[P]_{tit} = (3/5)10Ca_T + n_B P_T$$

Ca_T and P_T are the reaction concentrations of the respective ions in the working solution. Ca_{tit} and P_{tit} are the lattice ion titrant concentration, n_B is the number of burettes used (In this work $n_B = 2$; subscript T means total concentrations). The molar concentration ratio of the titrant corresponded to the stoichiom-

etry of the HAP phase, Ca/P/OH = 5:3:1. As a result, the HAP crystallization took place under conditions of constant supersaturation.[7),25)]

The crystals removed by filtration were examined by scanning electron microscopy (SEM), X-ray powder diffraction, FT–IR, and specific surface area.

3. Results and discussion

3.1 Kinetics of crystal growth

In seeded crystal growth experiments, the rate of crystallization is usually monitored by measuring the concentration of calcium ion as a function of time, following the introduction of seed crystals. The crystal growth rates, R_{HAP}, were determined from the slopes of the plots of titrant volume added as a function of time and is defined by Eq. (1).

$$R_{HAP} = dV/dt \quad (1)$$

where V is the volume of calcium chloride or potassium phosphate titrant added to solution. This rate must be converted in to moles of HAP precipitated per unit time;

$$R_{HAP} = dn/dt \quad (2)$$

where dn is the number of moles of solid HAP grown during the time dt. In order to calculate dn/dt, the solute titrant concentrations have to be corrected for dilution in the reaction solution, since each volume element added, dV, must be composed of supersaturated solution of identical lattice ion composition as the reaction medium. Application of the dilution correction results in following equations, for the rate of crystallization of HAP;

$$R_{HAP} = dV/dt\ C_{ET} = dn/dt \quad (3)$$

C_{ET} is the effective lattice ion titrant concentration, and is given by

$$C_{ET} = Ca_{tit} - n_B(Ca_T) \quad (4)$$

The crystallization rate, dn/dt, can be subsequently normalized for the mass and surface area of the crystals in reaction solution, by using Eq. (5)

$$R_{HAP} = \frac{dn}{m_{seed} SA_{seed} dt} \quad (5)$$

where m_{seed} is the mass, and SSA_{seed} is the specific surface area of the seed crystals in solution, respectively. The final equation is

$$R_{HAP} = \left(\frac{(dV/dt)C_{ET}}{m_{seed} SA_{seed}} \right) \quad (6)$$

where R_{HAP} is growth rate of HAP (mol/m^2 min), dV/dt is the rate of titrant added (mL/min), C_{ET} is effective titrant concentration (mol/mL), m_{seed} is the initial mass of the seed (g), and SA_{seed} is specific surface area of the seed crystals (m^2/g). Owing to the reduction of the specific surface area during crystallization, the rates were taken at titrant addition corresponding to precipitated HAP $\approx 5\%$, with respect to the added HAP seed crystal concentration.[26)]

The effect of polymer on the rate of crystallization was determined over a concentration range of 0.04×10^{-7} to 20×10^{-7} mol/L. The inhibitory activity of the additives was defined in terms of growth rate in the absence of additive, R_o, and the growth rate in the presence of additive, R_i. The experimental conditions and calculated results are given in **Table 2**.

Three CMI biopolymers with an average molecular weight of 2500 to 3000 Da were investigated under identical growth conditions. Table 2 summarizes the results obtained with the three CMI polymers used in this study and the effect of added polymer on the crystallization rate. It can be seen from Table 2 that an increase in polymer concentration results in a decrease of rate values. The decrease of rate values depends on the nature of the inhibitor and its effective concentration at a given condition.[27)–29)] It can be seen that even at considerable dilutions (0.04×10^{-7} mol/L), CMI-25, CMI-20 and CMI-15 reduced the growth rate of HAP by as much as 47, 38 and 7% respectively. The addition of CMI-25 to crystallization solution significantly reduced the growth rate of HAP. Addition of just 4×10^{-7} mol/L CMI-25 affords a reduction of the growth rate from 13.20×10^{-8} to 0.08×10^{-8} mol/m^2 min.

Table 2. Effect of carboxymethyl inulin on crystal growth of HAP at pH = 7.4; $Ca_T/P_T = 1.67$ and 37°C

Polymer	$C \times 10^7$ (mol/L)	$R_{HAP} \times 10^8$ (mol/m^2 min)
Blank	—	13.20
CMI-15	0.04	12.30
	0.40	9.70
	1.20	6.90
	12.00	5.00
	20.00	3.20
CMI-20	0.04	8.20
	0.20	7.20
	0.40	6.30
	1.20	3.50
	3.20	1.70
CMI-25	0.04	7.00
	0.20	6.10
	0.40	4.20
	0.80	3.00
	1.20	2.10
	4.00	0.08

Table 3. Experimental conditions for the crystallization of HAP on HAP seed crystals in the presence of 0.40×10^{-7} mol/L CMI-15 at pH 7.4; $Ca_T/P_T = 1.67$ and 37°C

$Ca_T \times 10^4$ (mol/L)	$R_{HAP} \times 10^8$ (mol/m^2 min)	σ
6	13.00	9.27
5	9.70	8.27
4	6.10	6.73
3	3.40	5.09

The relative solution supersaturation with respect to HAP, σ, is defined as,

$$\sigma = \frac{[IP^{1/9} - (K_{sp})^{1/9}]}{(K_{sp})^{1/9}} = S^{1/9} - 1 \quad (7)$$

in which IP is the ionic activity product and K_{sp} represent the thermodynamic solubility product and was taken as 4.7×10^{-59} mol^2/L^2 for HAP at 37°C. The ratio IP/K_{sp} represents the degree of supersaturation, S, and was computed by using MINEQL+ chemical equilibrium modeling software,[30)] which is free energy minimization program taking into account all equilibria in the solution, mass balance and electroneutrality conditions. The calculated growth rates and relative supersaturations, are given in **Table 3**.

The crystallization rates of sparingly soluble salts may be expressed in several ways, the most common of which is to write

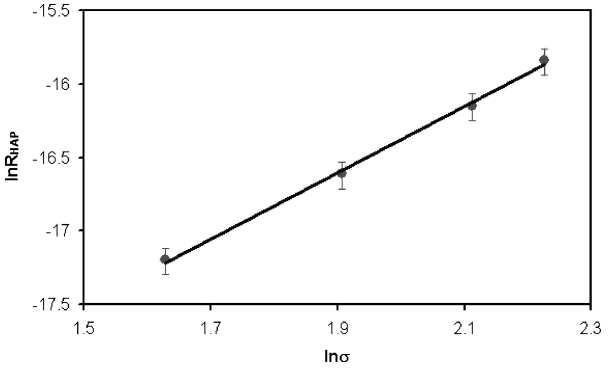

Fig. 2. Rate of crystallization of HAP on HAP seed.

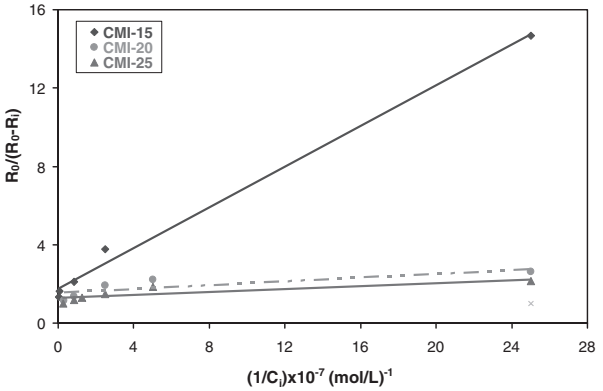

Fig. 3. Crystal growth of HAP on HAP seed crystals. Langmuir-type plot of HAP for biopolymers.

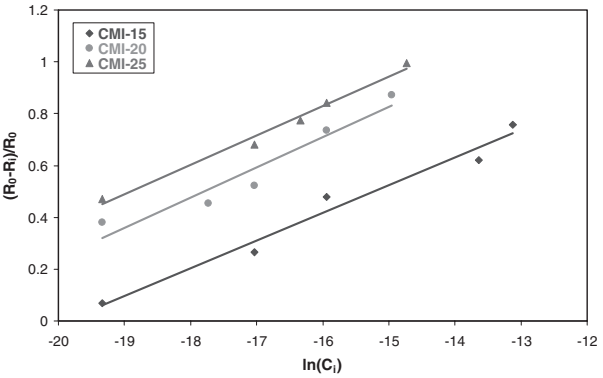

Fig. 4. Crystal growth of HAP on HAP seed crystals. Temkin-type plot of HAP for biopolymers.

the rate as a function of driving force. Nielsen suggested an empirical kinetic equation, which can indicate surface mechanism is dominant.[31)]

The rate of HAP crystallization can be expressed in terms of semiemprical kinetics equation:

$$R_{\mathrm{HAP}} = k\sigma^n \tag{8}$$

where k is the rate constant for crystal growth, n is the apparent order of the crystal growth. Logarithmic plots of the rates of HAP formation on HAP seed crystals as a function of the relative supersaturation yielded a straight line as shown in **Fig. 2**. The values of n are 1 for adsorbtion control, 2 for spiral growth and >2 for polynuclear growth. The value of n, the effective order of the reaction was found as 2.2 ± 0.2 for HAP growth in the presence of 0.40×10^{-7} mol/L CMI-15. When the deviation is taken into account, this value suggests a predominantly spiral dislocation, surface controlled process. This value in agreement with earlier reports on the seeded growth of HAP.[32)]

3.2 Adsorption mechanism

The polyelectrolyte is adsorbed on the crystal surface and effectively retards, or prevents further crystallization at very low concentrations. The effect of additives on morphology and growth rates of crystals has been discussed in many papers.[33)–36)] The theoretical models describing the effect of additives on crystallization processes are based on the concept of adsorption of additives, according to their nature, on different sites on the surface of the crystal. Cabrera and Vermileya (CV) considered theoretically the adsorption of impurities at kinks in steps and at the surface terraces.[37)] According to this model, growth inhibition is assumed to be accomplished through a fence of adsorbed inhibitor ions upon the smooth crystal surface. As pointed out by Vermileya, a step moving across the crystal surface will be stopped by the inhibitor. As the growth of various mineral salts has shown to be blocked when only a few percentage of the available crystal surface are covered with inhibitor ions, inhibition mechanism may be explained by preferential adsorption of the inhibitor at the active growth sites upon the surface. Cabrera and Vermileya described, based on the Burton–Cabrera–Frank (BCF) model, the pinning mechanism of an impurity due to the adsorption of inhibitors on faces. Since the amounts of polymer in solution were small, the inhibition could probably be attributed to the blocking of the active growth sites of the seed crystals.[38),39)] In the case of a spiral growth mechanism, the relationship between the relative growth rate R_i/R_0 and the fraction coverage, θ_i of the surface in the presence of impurity may be given by.[40)–42)]

$$\left(\frac{R_0 - R_i}{R_0}\right)^n = \alpha^n \theta_i \tag{9}$$

The exponent $n = 1$ represents the case at which impurity adsorption occurs at kinks in step edges as in Kubota–Mullin model. θ_i is the coverage of adsorption-active sites and may be described by the Langmuir and Temkin adsorption isotherms;

$$\theta_i = \frac{KC_i}{1 + KC_i} \quad \text{Langmuir isotherm} \tag{10}$$

$$\theta_i = Z \ln C_0 + Z \ln C_i \quad \text{Temkin isotherm} \tag{11}$$

where K, C_0, Z are constants and C_i is the additive concentrations. Using Eq. (9) in combination with the Langmuir and Temkin isotherm (Eqs. (10)–(11)) we can write the following equations, linear in $(1/C_i)$ and $\ln(C_i)$

$$\frac{R_0}{R_0 - R_i} = \alpha^{-1}\left(1 + \frac{1}{KC_i}\right) \quad \text{Langmuir isotherm} \tag{12}$$

$$\frac{R_0 - R_i}{R_0} = z\alpha(\ln C_0 + \ln C_i) \quad \text{Temkin isotherm} \tag{13}$$

Our kinetic data were fitted to Eqs. (12) and (13) to check the validity of models (**Figs. 3** and **4**). Figure 3 illustrates the plots of $R_0/(R_0 - R_i)$ against C_i^{-1} while Fig. 4, presents the plots of $(R_0 - R_i)/R_0$ against $\ln(C_i)$.

Equation (12) shows that this model predicts a linear relationship between $R_0/(R_0 - R_i)$ and $1/C_i$. In many instances, the influence of the surface adsorbed inhibitors on crystallization is not adequately described by Eq. (12). This phenomenon is also observed in our experimental results. This is probably the result

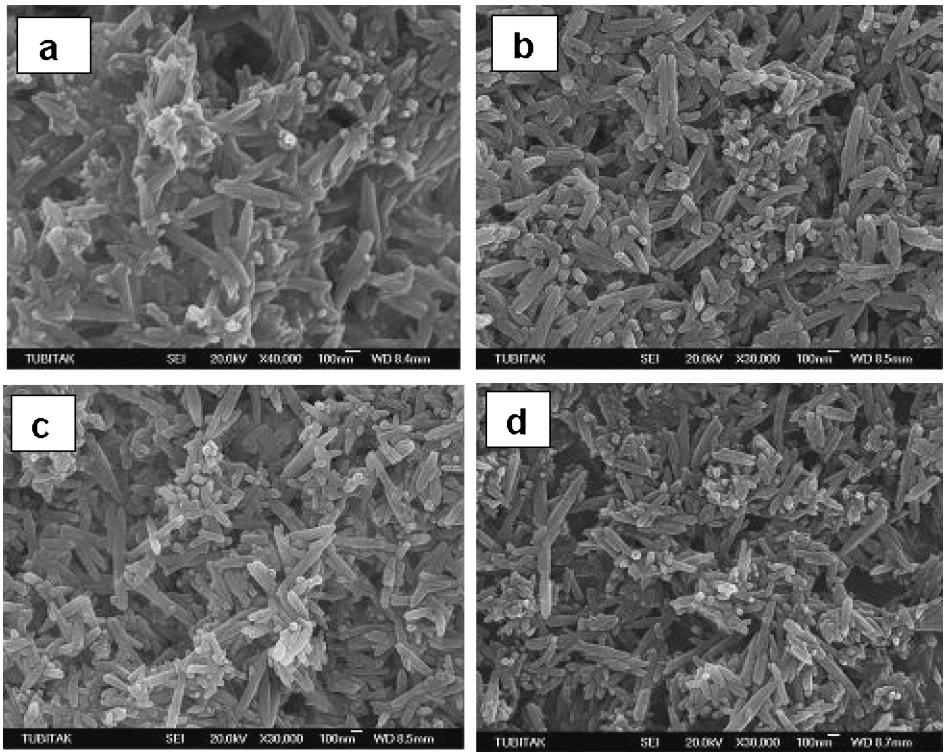

Fig. 5. SEM of (a) control (b) crystals grown from a solution containing 0.40×10^{-7} mol/L CMI-15 (c) crystals grown from a solution containing 0.40×10^{-7} mol/L CMI-25 (d) crystals grown from a solution containing 12×10^{-7} mol/L CMI-15.

Table 4. The properties of HAP crystals grown from a solution containing 0.40×10^{-7} mol/L biopolymers

Samples	L_{002} (nm)	L_{300} (nm)	L_{002}/L_{300}	L^a (nm)	SD^c	W^a (nm)	SD^c	L/W
HAP control	83	30	2.8	343	±113.3	74	±16.9	4.64
CMI15	57	54	1.1	304	±94.7	66	±10.1	4.61
CMI15^b	—	—	—	238	±75.9	64	±12.3	3.65
CMI20	44	45	0.98	—	—	—	—	—
CMI25	43	44	0.98	227	±87.9	62	±12.7	3.66

^{a}SEM results. $^b12 \times 10^{-7}$ mol/L biopolymer. ^{c}SD = standard deviation

of deviations from ideality in the adsorpsion equilibria of inhibitor molecules onto the nearly saturated crystal surfaces. In these cases, the implicit assumptions of the Langmuir adsorption model, i.e. that a) the surface is composed of uniform adsorption sites and b) no interactions occur between adsorbent molecules, are probably oversimplified. On the other hand the linearity of the plots of Eq. (13) for HAP crystal growth in the presence of biopolymer (Fig. 4) suggests that the mechanism of the inhibitory effect of polymer best follows the Temkin model.

3.3 Effect of the biopolymers on the crystal morphology

Photographs were also taken by scanning electron microscope (SEM) for the subsequent visual analysis in order to asses the effects of polymers on crystal shape and size. The morphologies of the HAP powders from SEM investigation are shown in **Fig. 5**. They are formed of agglomerated particles of a needle-like morphology. The dimensions of minimum of 75 crystals in each sample were measured from SEM photomicrographs. The average value of the length L where L is parallel to the c-axis and the average value of the width (W) and aspect ratio (i.e., L/W) are given in **Table 4**. The crystals precipitated at 37°C have the form of tiny needles with average length of around 343 nm and width of 74 nm in the absence of polymers (Fig. 5a). The size distribution of the control sample is shown in **Fig. 6**a. The length distribution of the control sample is broad (Fig. 6a) The presence of polymers in supersaturated solutions affects not only the kinetics of crystal growth but crystal size as well. Figure 5 shows the effect of polymers on crystal habit. No apparent changes in morphology were observed in the presence of polymers. The precipitated crystals show similar needlelike shape. The average length and width of the crystals grown in the presence of the polymers was less than that of the control sample (Figs. 5(b–d)). The average length of the crystals was reduced to 304 nm and 227 nm for solution containing 0.40×10^{-7} mol/L CMI-15 and CMI-25 respectively. The average width of the crystals was reduced to 66 and 62 nm for solution containing 0.40×10^{-7} mol/L biopolymer. Figure 6c shows the length distribution as affected by the polymer. Biopolymer yields crystals with a fairly narrow size distribution compared to control sample. The decrease of the length of the distribution of the crystals as the polymer is added hints for a retardation of crystal growth more in the axial direction. As can be seen in Table 4 aspect ratio of the crystals decreased in the presence of polymers. An increase in polymer concentration resulted in decrease in the size of the HAP crystals. The average size of the HAP crystals decreased from

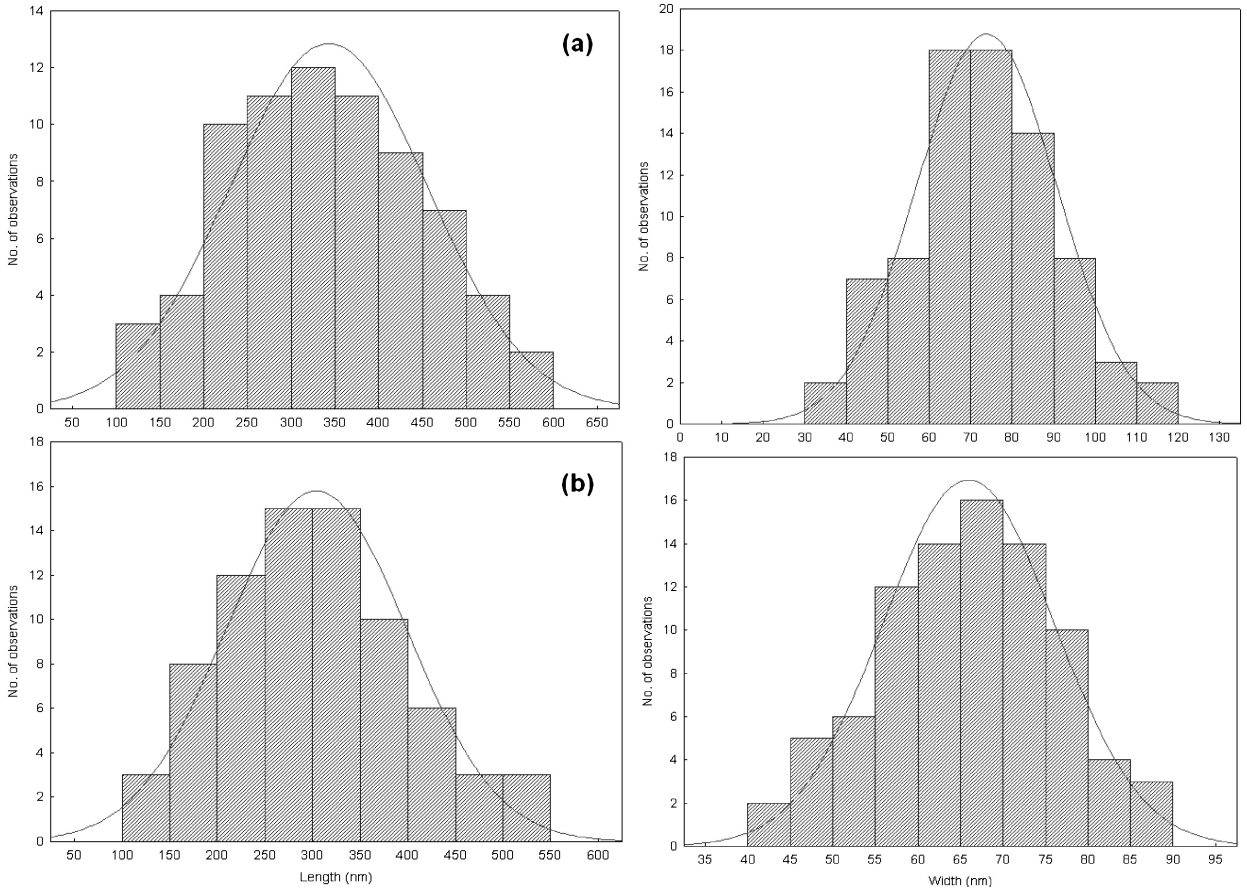

Fig. 6. Length and width of (a) control (b) crystals grown from a solution containing 0.40×10^{-7} mol/L CMI-15.

304 to 238 nm as the CMI-15 concentration increased from 0.40×10^{-7} to 12×10^{-7} mol/L. These results showed that polymers tested in this study are effective as growth inhibitors in this experimental condition.

XRD spectra of all samples have shown peaks characteristic for HAP (**Fig. 7**). The principal diffraction peaks of HAP appear at 2θ values of 25.88° for reflection (002), at 31.77° for reflections (211), and at 32.90° for reflection (300).

The peak broadening of XRD reflection can be used to estimate the crystallite size in a direction perpendicular to the crystallographic plane based on Scherrer's equation as follows:[43)]

$$L_{hkl} = \frac{k\lambda}{B\cos\theta} \tag{14}$$

where L_{hkl} is the mean crystallite size in nm, k is the shape factor, B is the broadening of the diffraction line measured at half of its maximum intensity. B was determined by full width at half maximum (FWHM) middle point method. The shape factor k becomes 0.9 when FWHM is used for B. λ is the wavelength of X-ray and θ is the Bragg diffraction angle. By using Scherrer equation and half width of diffraction peaks for HAP, crystallite size of each specimen is listed in Table 4. Based on the structure investigation, the size of the individual HAP crystals was calculated from the broadening 002 and 300 diffraction peaks, assuming that HAP crystals were hexagonal rode like prisms whose height is equal to the crystallite size along the 002 plane (c-axis) and a length of the rode corresponds to the crystallite size along the 300 plane (a-axis) (Table 4).

The results showed that a L_{002} values of HAP sample are reduced in the presence of polymers. The size of the crystallites

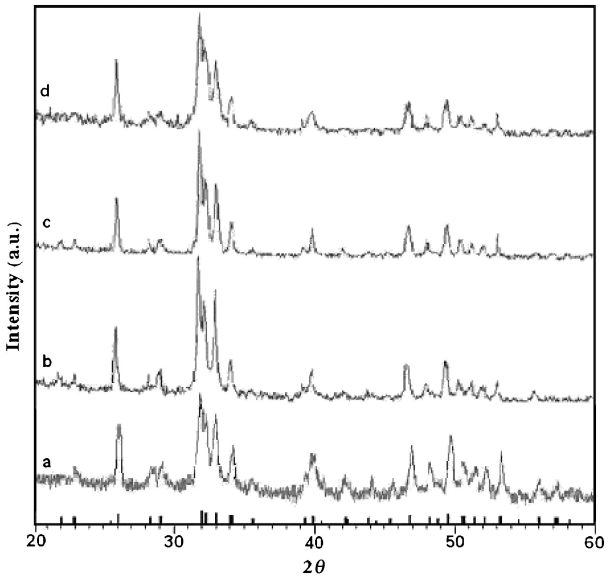

Fig. 7. X-ray diffraction spectra of HAP samples in the absence and in the presence of polymers. (a) control; (b) crystals grown from a solution containing 0.40×10^{-7} mol/L CMI-15; (c) crystals grown from a solution containing 0.40×10^{-7} mol/L CMI-20; (d) crystals grown from a solution containing 0.40×10^{-7} mol/L CMI-25.

responsible for the Bragg reflection (002) and (300) planes were 83 nm and 30 nm respectively in the absence of polymers. The (c) axis direction was about 2.8 times longer than (a) axis direction

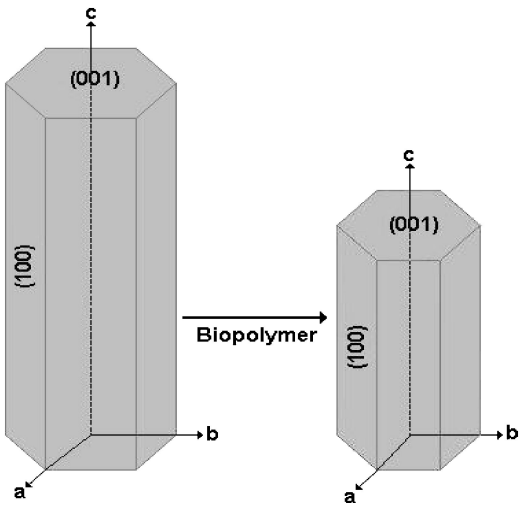

Fig. 8. Schematic representation of the influence of biopolymer on HAP crystals.

(L_{002}/L_{300}) and anisotropy decreases in the presence of polymers (Table 4). Biopolymer promoted a decrease in the aspect ratio (L/W) relative to growth in the absence of polymer, XRD and SEM results showed that polymer causes a retardation of crystal growth more in the axial direction (c-axis of the lattice) than in the radial direction. The schematic representation of the hydroxyapatite morphology along the [001] axis and the influence of biopolymer on HAP crystals are shown in **Fig. 8**. HAP has a hexagonal structure with a space group of $P6_3/m$ and unit cell contains 10 calcium atoms, 6 phosphate and 2 hydroxide groups. Generally, the crystal forms display a needle-like morphology. It is reported that the calcium surface concentration of the HAP on the (001) face is greater than that on the (100) face. Therefore (001) face will be charged positively and (100) face will be charged negatively as a result of the the enrichment of plane with hydroxyl and phosphate groups.[44] This result implies that the (001) face can adsorb a higher number of carboxylate moieties from the polymers. Therefore the interactions between polymer and the HAP (001) faces resulted in a gradual decrease in length of the crystal with increasing carboxylation degree of the CMI and polymer concentration. Apparently the larger number of carboxylate functional groups increase the ionic attractive interactions between the adsorbate ($-COO^-$) and the positive sites (Ca^{2+}) at surface. The first step in polymer action, as proposed by Addadi and Weiner is sharing of Ca^{2+} ions with crystal surface.[45] Only the growth of those crystal faces, however, where at least one set of carboxylate groups in the crystal lattice is oriented perpendicular to the crystal surface is retarded. The polymer backbone forms a fence at the crystal surface, thus hampering the step propagation. Biologically, the inhibitory effects on the (001) face are more important than that on the (100) face since biological HAP grows mainly in the c-axis direction.[46]

4. Conclusions

Biopolymers tested in this study are effective as growth inhibitors of HAP under the described experimental conditions. The higher affinity of CMI-25 for HAP crystal surfaces is reflected on the more profound effect of CMI-25 on the HAP crystal growth rate. CMI-25 polymeric chains have a higher anionic charge density because they contain a higher number of carboxyl groups compared to CMI-15 or CMI-20. Therefore, they mitigate the interaction ability of the appended anionic $-COO^-$ groups with the solid phase. The polymer backbone can then act as a "fence" on the crystal surface, thus forming an obstacle for propagating steps that lead to further crystal growth.

All the results of the present investigation indicate that, anionic biopolymers can inhibit hydroxyapatite crystal growth and that such inhibition is directly linked to fractional coverage of adsorption sites. The degree of inhibition of hydroxyapatite crystallization by CMI biopolymers is related to the maximum surface charge density due to adsorbed polymer.

From a physicochemical point of view, efficient regulators of calcification would be those molecules that have a high enough adsorption affinity so that low concentrations can result in the adsorption on and blocking of a significant number of crystal growth sites on the crystallites of the tissue.

Acknowledgements We appreciate the support of YTU B.A.P.K. (Project No: 22-07-01-01); DPT (Project No: 25-DPT-07-04-01 and Project No: 24-DPT-07-04-01) for the accomplishment of this work.

References

1) P. G. Koutsoukos, Z. Amjad, M. B. Tomson and G. H. Nancollas, *J. Am. Chem. Soc.*, 102, 1553–1557 (1980).
2) S. Koutsopoulos and E. Dalas, *J. Colloid Interface Sci.*, 231, 207–212 (2000).
3) Z. Amjad, *J. Colloid Interface Sci.*, 117, 98–103 (1987).
4) M. Öner and Ö. Dogan, *Prog. Cryst. Growth Charact. Mater.*, 50, 39–51 (2005).
5) Ö. Dogan and M. Öner, *Langmuir*, 22, 9671–9675 (2006).
6) P. G. Koutsoukos, Z. Amjad and G. H. Nancollas, *J. Colloid Interface Sci.*, 83, 599–605 (1981).
7) M. Dalpi, E. Karayianni and P. G. Koutsoukos, *J. Chem. Soc., Faraday Trans.*, 89, 965–969 (1993).
8) B. M. Chesnutt, Y. Yuan, K. Buddington, W. O. Haggard and J. D. Bumgardner, *Tissue Eng., Part A*, 15, 2571–2579 (2009).
9) M. Sedlak and H. Colfen, *Macromol. Chem. Phys.*, 202, 587–597 (2001).
10) Ö. Dogan and M. Öner, *J. Nanosci. Nanotechnol.*, 8, 667–674 (2008).
11) G. H. Nancollas and W. Wu, *J. Cryst. Growth*, 211, 137–142 (2000).
12) S. Mann, D. D. Archibald, J. M. Didymus, T. Douglas, B. R. Heywood, F. C. Meldrum and N. J. Reeves, *Science*, 261, 1286–1292 (1993).
13) M. Öner, Ö. Dogan and G. Öner, *J. Cryst. Growth*, 186, 427–437 (1998).
14) M. Öner, J. Norwig, W. H. Meyer and G. Wegner, *Chem. Mater.*, 10, 460–463 (1998).
15) D. L. Verraest, J. A. Peters, H. van Bekkum and G. M. van Rosmalen, *J. Am. Oil Chem. Soc.*, 73, 55–60 (1996).
16) R. Berends and H. C. Kuzee, Process for Controlling Scale in The Sugar Process, European Patent Specification EP 1 060 135 B1 (2001).
17) D. L. Verraest, J. G. Batelaan, J. A. Peters and H. van Bekkum, Carboxymethyl Inulin, United States Patent 5,777,090 (1998).
18) B. Akın, M. Öner, Y. Bayram and K. D. Demadis, *Cryst. Growth Des.*, 8, 1997–2005 (2008).
19) K. D. Demadis, E. Mavredaki, E. N. Stathoulopoulou and C. Mantzaridis, *Desalination*, 213, 38–46 (2007).
20) D. L. Verraest, J. A. Peters, J. G. Batelaan and H. Van Bekkum, *Carbohydr. Res.*, 271, 101–112 (1995).
21) C. V. Stevens, A. Meriggi and K. Booten, *Biomacromolecules*, 2, 1–16 (2001).
22) F. R. Johannsen, *Food Chem. Toxicol.*, 41, 49–59 (2003).
23) J. Zhang, A. Ebrahimpour and G. Nancollas, *J. Colloid Interface Sci.*, 152, 132–140 (1992).

24) E. Dalas, J. K. Kallitsis and P. G. Koutsoukos, *Langmuir*, **7**, 1822–1826 (1991).
25) P. G. Koutsoukos, Ph.D. Thesis, State University of New York (1980).
26) S. Koutsopoulos and E. Dalas, *J. Cryst. Growth*, **216**, 443–449 (2000).
27) Z. Amjad, *Langmuir*, **3**, 1063–1069 (1987).
28) V. K. Sharma, M. Johnsson, J. D. Sallis and G. H. Nancollas, *Langmuir*, **8**, 676–679 (1992).
29) Z. Amjad, *Can. J. Chem.*, **67**, 850–856 (1989).
30) MINEQL+, Chemical Equilibrium Modeling System, version 4.0.
31) A. E. Nielsen, "Kinetics of Precipitation," Macmillan Co., New York (1964).
32) E. Dalas and A. Chrissanthopoulos, *J. Cryst. Growth*, **255**, 163–169 (2003).
33) M. C. Van der Leeden and G. M. van Rosmalen, *J. Cryst. Growth*, **100**, 109–116 (1990).
34) M. C. Van der Leeden, D. Kashchiev and G. M. van Rosmalen, *J. Cryst. Growth*, **130**, 221–232 (1993).
35) R. J. Davey, *J. Cryst. Growth*, **34**, 109–119 (1976).
36) M. P. C. Weijnen and G. M. van Rosmalen, *J. Cryst. Growth*, **82**, 528–542 (1987).
37) N. Cabrera and D. A. Vermileya, "Growth and Perfection of Crystals," 3rd ed., Wiley, New York (1958) p. 393.
38) S. T. Liu and G. H. Nancollas, *J. Colloid Interface Sci.*, **52**, 582–592 (1975).
39) Z. Amjad, *Colloids Surf.*, **48**, 95–106 (1990).
40) N. Kubota and J. W. Mullin, *J. Cryst. Growth*, **152**, 203–208 (1995).
41) K. Sangwal, *Prog. Cryst. Growth Charact. Mater.*, **36**, 163–248 (1998).
42) K. Sangwal, *J. Cryst. Growth*, **203**, 197–212 (1999).
43) B. D. Cullity, "Elements of X-Ray Diffraction," 2nd ed., Addison-Wesley Publishing Company, Reading, MA (1978).
44) I. S. Neira, Y. V. Kolenko, O. I. Lebedev, G. Van Tendeloo, H. S. Gupta, F. Guitan and M. Yoshimura, *Cryst. Growth Des.*, **9**, 466–474 (2009).
45) L. Addadi and S. Weiner, *Proc. Natl. Acad. Sci. U.S.A.*, **82**, 4110–4114 (1985).
46) E. Bertoni, A. Bigi, G. Falini, S. Panzavolta and N. Roveri, *J. Mater. Chem.*, **9**, 779–782 (1999).